# Consistent description of hindrance in sub-barrier fusion of $^{48}$Ca with $^{36}$S, $^{48}$Ca, and $^{96}$Zr

Şerban Mişicu* and Florin Carstoiu
*Department for Theoretical Physics, National Institute for Physics and Nuclear Engineering-Horia Hulubei, P.O. Box MG6, Bucharest-Magurele, Romania*
(Received 8 April 2011; published 31 May 2011)

Recent fusion reaction data for the systems $^{36}$S + $^{48}$Ca, $^{48}$Ca + $^{48}$Ca, and $^{96}$Zr + $^{48}$Ca are analyzed within the coupled-channel formalism. The heavy-ion entrance channel potential is calculated employing an improved double-folding prescription. The nonlocal kernel arising from the knock-on exchange component of the effective $N$-$N$ interaction is localized within the lowest order of the Perey-Saxon approach, including full recoil. The single-particle densities entering the folding integrals are prescribed according to the density matrix expansion method. The investigation is more elaborated because each case is tested with four different types of $N$-$N$ effective forces: The two standard parametrizations of the density-independent M3Y force (Reid and Paris) and two parametrizations of the density-dependent Gogny force (D1S and D1N). A consistent description of all three reactions is achieved by keeping fixed the nuclear structure input for $^{48}$Ca. The inclusion of $2^+$ and $3^-$ phonon states in the coupled-channel calculation, within an energy excitation window identical for all three reactions explains better the hindrance in extreme sub-barrier fusion cross sections. The interactions providing the best fit to the data are not pointing to a possible maximum in the astrophysical $S$ factor, thereby confirming the conclusion reached by the Legnaro group for these cases.

DOI: 10.1103/PhysRevC.83.054622 PACS number(s): 25.70.Jj, 24.10.Eq, 25.60.Pj

## I. INTRODUCTION

Very recently the fusion excitation function of $^{36}$S + $^{48}$Ca was experimentally investigated at Legnaro and cross sections as low as ≈600 nb were attained [1]. Along with this case the Legnaro group reinvestigated the system $^{48}$Ca + $^{48}$Ca down to ≈500 nb [2]. The cross sections reported earlier for this last case were revised by a 0.8 renormalization factor [3]. These authors remarked that although the logarithmic derivative (slope) after a sharp increase below the Coulomb barrier saturates (level off), these two reactions still bear hindrance features. This conclusion is in disagreement with Jiang *et al.*, who analyzed several other projectile-target combinations [4] displaying hindrance. According to these authors a signature for the onset of hindrance is the apparent occurrence of a maximum in the $S$ factor and consequently a steep increase of the slope well below the Coulomb barrier. To explain the data, Stefanini *et al.* [1,2] assumed a large diffuseness parameter ($a = 0.9$ fm) in the Akyüz-Winther (AW) potential that is customarily used in the coupled-channel (CC) analysis of medium-heavy nuclei fusion data. For the reaction $^{96}$Zr + $^{48}$Ca reported earlier by the Legnaro group the same conclusion was reached, that is, a probable saturation of the slope and the need for a large diffuseness to explain the data [5].

In a very recent publication [6] the Legnaro group reported measurements on a new medium-light system, $^{36}$S + $^{64}$Ni, and showed that an even larger diffuseness parameter ($a = 1.2$ fm) is necessary to fit the data. The assumption of an abnormally large diffuseness of the potential was used earlier in Ref. [7] to explain the large slope at deep sub-barrier energies for the case $^{58}$Ni + $^{58}$Ni. Very recently the same authors speculated that the conjecture of a large surface diffuseness $a$ for fusion below the barrier and a smaller (but still large) value above the barrier is consistent with the special nature of octupole phonon states in nuclei with closed neutron and/or proton shells [8]. However, the systematic analysis [9] of fusion at energies over the barrier found diffuseness much larger than the value $a = 0.65$ needed to reproduce elastic scattering data, suggesting the inadequacy of the Woods-Saxon shapes to describe fusion cross section.

In a series of papers [10–14] a different explanation of the hindrance phenomenon occurring in several medium-light and medium-heavy systems was given. The basic idea consists of using a heavy-ion potential modified in such a manner that a strong overlap between the nuclear-matter distribution tails of the projectile and target is prevented. For such configurations, especially in the inner part of the barrier, additionally to the standard direct and exchange components of the ion-ion potential, a strongly repulsive potential is acting. Its strength is fixed by requiring that for total overlap of two nuclei the increase in the nuclear potential is provided by the variation of the symmetric nuclear matter equation of state from normal density to twice the normal density, as formerly considered for the case of giant trinuclear molecules [15].

There is also another proposal put forward in last time to solve the hindrance puzzle. In a recent work [16] good fits for only two cases were reported: $^{64}$Ni + $^{64}$Ni and $^{16}$O + $^{208}$Pb. Although it was stressed that the approach is essentially different from the dynamical approach of Ref. [10], the basic ingredients necessary to reproduce the data include a Coulomb barrier that, similarly to the one used in Ref. [10], is much thicker than the traditional Akyüz-Winther prescription, and the same CC approach was used for the cross-section calculations. To date there is no other mechanism capable of describing with a similar accuracy

*misicu@theor1.theory.nipe.ro [http://theor1.theory.nipne.ro/∼misicu/].

 

the data simultaneously in the low- and high-energy sectors of systems displaying hindrance in sub-barrier fusion. For example, Ref. [17], reporting the fusion cross sections at deep sub-barrier energies for the reaction $^{16}O + ^{208}Pb$, presented also calculations within the standard CC formalism which failed to reproduce simultaneously the new and the old data. In that paper it was argued that a new approach, rooted in the theory of a quantum open system, is needed to describe the hindrance to fusion. Despite later theoretical developments in this direction, the quantum decoherence approach was not applied to systems classified as displaying inhibition to fusion. The microscopic study of Ref. [18] underscored the fact that the fusion excitation function of the reaction $^{16}O + ^{208}Pb$ is extremely sensitive to the energy dependence of the potential barrier. Therefore, an optimal energy should be guessed to adequately describe the data. Even so, once a good description is achieved for the lowest experimental points, the data are grossly underestimated in the high-energy sector.

In what follows we focus our analysis on the three fusion reactions, mentioned in the first paragraph of this section, and demonstrate that the data can be described by using exactly the same nuclear structure input for $^{48}Ca$. For the other two nuclei the nuclear structure input used in the present work is close to the one used by Stefanini *et al.* for $^{36}S$ in Ref. [1] and $^{96}Zr$ in Ref. [5] (similar also in the theoretical analysis of Ref. [19]).

The paper is organized as follows: We discuss first the details allowing the computation of the heavy-ion potential, such as single-particle densities, nucleon-nucleon ($N$-$N$) effective forces, and the calculation of the exchange part of this potential. Regarding the last two issues we introduced modifications and extensions compared to our previous papers. There the double-folding potential was computed via the M3Y interaction with Reid soft-core $G$-matrix elements in the even channels and Elliott soft-core $G$-matrix elements in the odd channels (abbreviated M3Y-Reid), and the exchange part, which dominates this interaction, was treated in the most simple approximation: a zero-range pseudopotential $\hat{J}_0\delta(\boldsymbol{r})$ with an energy-independent strength. In the present study we employ a localization procedure on the nonlocal exchange kernel, calculated in the knock-on approximation. As for the effective forces we use a broader set of interactions. Apart of the M3Y-Reid parametrization used earlier, we introduce also the $G$-matrix interaction based on Paris $N$-$N$ potential (abbreviated M3Y-Paris) and the Gogny force with two of its best parametrizations, D1S and D1N. In Sec. III we present the results of the CC calculations using these various types of potentials for all three reactions and display the quantities relevant for the sub-barrier fusion analysis such as cross sections in logarithmic and linear scales, astrophysical $S$ factors, and logarithmic derivatives. We also attempt to offer an explanation for the similar scaling between the logarithmic derivatives of the systems $^{36}S + ^{48}Ca$ and $^{48}Ca + ^{48}Ca$ as a function of the cross section. We conclude the paper in Sec. IV by stressing the similarities and differences between the three investigated reactions and the ability of the employed interactions to describe the data.

## II. HEAVY-ION POTENTIAL

We compute the entrance channel heavy-ion potential for fusion reactions within the double-folding model. This method has the advantage of incorporating nuclear structure effects (neutron and proton matter distribution), as well as details of the nucleon-nucleon effective interactions.

We take for the nuclear-matter density a simple Fermi-Dirac function,

$$\rho(r) = \frac{\rho_0}{1 + \exp[(r - c)/a]}, \tag{1}$$

where

$$\begin{aligned} &a = 0.540\,\text{fm}, \quad c = 3.40\,\text{fm}\ (^{36}S), \\ &c = 3.75\,\text{fm}\ (^{48}Ca), \quad c = 4.83\,\text{fm}\ (^{96}Zr). \end{aligned} \tag{2}$$

The parameter $\rho_0$ is determined through normalization:

$$\rho_0 = \frac{3A}{4\pi c^3(1 + \pi^2/c^2)}.$$

The values chosen above for the half radius $c$ are consistent within 2% with the values chosen by Negele [20] to fit the rms radii of the charge distribution, that is, $c = 3.45$ fm for $^{36}S$, $c = 3.83$ fm for $^{48}Ca$, and $c = 4.91$ fm for $^{96}Zr$. With this choice the calculated rms radii are 3.311 fm for $^{36}S$, 3.531 fm for $^{48}Ca$, and 4.246 fm for $^{96}Zr$. These values compare well with the experimental values from the compilation [21]. The proton and neutron distributions are assumed to be sufficiently similar; therefore, we take

$$\rho_p(r) = \frac{Z}{A}\rho(r), \quad \rho_n(r) = \frac{N}{A}\rho(r). \tag{3}$$

In previous articles [10–14] we carried out the analysis of fusion in medium-light and medium-heavy systems using the Reid parametrization of the M3Y effective $N$-$N$ interaction as described originally by Bertsch *et al.* [22]. In Ref. [23] we employed the M3Y-Paris parametrization [24] and the Gogny force in the D1 parametrization to answer the conjecture put forward earlier by Jiang *et al.* [25] on the possible fingerprints of hindrance in the sub-barrier fusion reactions: $^{12}C + ^{12}C$, $^{12}C + ^{16}O$, and $^{16}O + ^{16}O$. The result was that there is essentially no difference between the two forces with respect to the data fit quality although one is appropriate for nuclear reactions, whereas the other was designed originally to describe nuclear ground state properties.

Below we extend our analysis to both Reid and Paris parametrizations of the M3Y interaction and two out of three parametrizations of the standard Gogny force. The parametrization D1S was designed to provide a better description of nuclear ground- and excited-state properties and reproduce nuclear fission barriers [26]. The D1N parametrization was very recently proposed to reproduce the neutron-matter equation of state much better than the D1S parametrization [27]. For this last force it was also found that the binding energies drift is diminished for the major part of isotopic chains. Neglecting the spin-orbit term, because we investigate reactions with spin-saturated nuclei, the Gogny interaction can be expressed as a sum of a central, finite-range term and a

zero-range density-dependent term:

$$v(\boldsymbol{r}_{12}) = \sum_{i=1}^{2}(W_i + B_i P_\sigma - H_i P_\tau - M_i P_\sigma P_\tau)e^{-\frac{r_{12}^2}{\mu_i^2}} + t_3(1+P_\sigma)\rho^\alpha(\boldsymbol{R}_{12})\,\delta(\boldsymbol{r}_{12}). \quad (4)$$

Above

$$\boldsymbol{r}_{12} = \boldsymbol{r}_1 - \boldsymbol{r}_2 \quad \boldsymbol{R}_{12} = \tfrac{1}{2}(\boldsymbol{r}_1 + \boldsymbol{r}_2),$$

and the representation of the interaction is given in terms of spin, $P_\sigma$, and isospin, $P_\tau$, exchange operators. The isoscalar and isovector direct and exchange components are given by

$$v_{00}^{\rm d} = \frac{1}{4}\sum_{i=1}^{2}(4W_i + 2B_i - 2H_i - M_i)e^{-r_{12}^2/\mu_i^2} + \frac{3}{2}t_3\,[\rho(\boldsymbol{R}_{12})]^\alpha\,\delta(\boldsymbol{r}_{12}), \quad (5)$$

$$v_{01}^{\rm d} = -\frac{1}{4}\sum_{i=1}^{2}(2H_i + M_i)e^{-r_{12}^2/\mu_i^2}, \quad (6)$$

$$v_{00}^{\rm ex} = -\frac{1}{4}\sum_{i=1}^{2}(W_i + 2B_i - 2H_i - 4M_i)e^{-r_{12}^2/\mu_i^2} - \frac{3}{4}t_3\rho^\alpha(\boldsymbol{R}_{12})\delta(\boldsymbol{r}_{12}), \quad (7)$$

$$v_{01}^{\rm ex} = -\frac{1}{4}\sum_{i=1}^{2}(W_i + 2B_i)e^{-r_{12}^2/\mu_i^2} - \frac{3}{4}t_3\rho^\alpha(\boldsymbol{R}_{12})\delta(\boldsymbol{r}_{12}). \quad (8)$$

The strengths of the interaction, $W$, $B$, $H$, $M$, $t_3$, and the exponent $\alpha$ are given in Ref. [26] for the D1S parametrization and in Ref. [27] for D1N. The overlap density is evaluated according to the prescription of Campi and Sprung [28],

$$\rho(R) = \sqrt{\rho_1\left(\boldsymbol{R} - \tfrac{1}{2}\boldsymbol{s}\right)\rho_2\left(\boldsymbol{R} + \tfrac{1}{2}\boldsymbol{s}\right)}, \quad (9)$$

where $\boldsymbol{s} = \boldsymbol{R} + \boldsymbol{r_1} - \boldsymbol{r_2}$ is the separation distance between the interacting nucleons.

The antisymmetrization of the matrix element of the interaction, required by the Pauli principle, is performed by retaining only the knock-on exchange term. Then the effective $N$-$N$ force reads

$$v(\boldsymbol{r}) = v^{\rm d}(\boldsymbol{r}) + v^{\rm ex}(\boldsymbol{r})P_{12}^x, \quad (10)$$

where $P_{12}^x$ exchanges the spatial coordinates of the interacting nucleons (knock-on exchange operator in coordinate space). In other words, the one-nucleon exchange knock-on term is assumed to be dominant with respect to all other exchange contributions. Because the range of nonlocality is small, the local equivalent of the nonlocal kernel corresponding to the finite range component of $v^{\rm ex}$ is obtained in the lowest order of the Perey-Saxon approximation [29]:

$$U_L(R) = 4\pi\int\rho_1(X)\rho_2(|\boldsymbol{R}-\boldsymbol{X}|)d\boldsymbol{X}\int v^{\rm ex}(s)\hat{j}_1\left(\hat{k}_1(X)\frac{A_1-1}{A_1}s\right) \cdot\hat{j}_1\left(\hat{k}_2(|\boldsymbol{R}-\boldsymbol{X}|)\frac{A_2-1}{A_2}s\right)j_0[K(R)s/\mu]s^2ds. \quad (11)$$

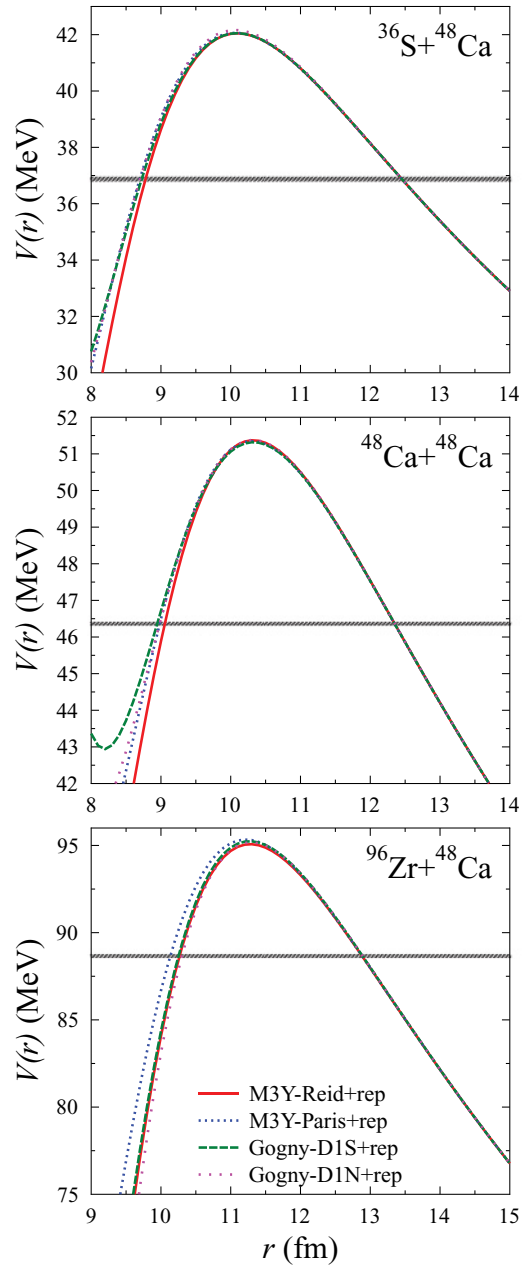


FIG. 1. (Color online) Ion-ion potentials for the systems $^{36}$S + $^{48}$Ca, $^{48}$Ca + $^{48}$Ca, and $^{96}$Zr + $^{48}$Ca using the M3Y (Reid and Paris) and Gogny (D1S and D1N) parametrizations. The dashed line corresponds to the lowest energy attained in experiment.

Above, the function $\hat{j}_1(x) = 3j_1(x)/x$ arises from the Slater approximation to the mixed density and includes correction from the nucleon recoil and $K(R)$ is the usual WKB local momentum for the relative motion,

$$K^2(R) = \frac{2\mu}{\hbar^2}[E - U_D(R) - U_L(R)]. \quad (12)$$

Note that $U_D$ above includes the Coulomb component $U_C$, which is calculated by folding the charge densities with the usual $v_C(r) = e^2/r$. In the extended Thomas-Fermi

TABLE I. Parameters of the heavy-ion potential for $^{48}$Ca + $^{48}$Ca: radii of the densities (1), radius $c_{\rm rep}$ and diffuseness $a_{\rm rep}$ of the modified densities, strength of the repulsive interaction $V_{\rm rep}$, minimum of the potential pocket $V_{\rm min}$, and Coulomb barrier height $V_{\rm bar}$.

| Interaction | $c$ (fm) | $c_{\rm rep}$ (fm) | $a_{\rm rep}$ (fm) | $V_{\rm rep}$ (MeV) | $V_{\rm min}$ (MeV) | $V_{\rm bar}$ (MeV) |
|---|---|---|---|---|---|---|
| M3Y-Reid | 3.75 | 3.93 | 0.472 | 6283.8 | 32.76 | 51.37 |
| M3Y-Paris | 3.75 | 3.93 | 0.466 | 6645.8 | 38.05 | 51.35 |
| D1S | 3.75 | 3.93 | 0.468 | 13263. | 42.94 | 51.32 |
| D1N | 3.75 | 3.93 | 0.465 | 13816.7 | 40.97 | 51.38 |

approximation the "local Fermi momentum" is defined by [30]

$$\hat{k}^2(r) = \left[\frac{3}{2}\pi^2\rho(r)\right]^{2/3} + \frac{5C_s[\nabla\rho(r)]^2}{3\rho(r)^2} + \frac{5\Delta\rho(r)}{36}, \qquad (13)$$

where $C_s \approx 0.25$ seems to be the appropriate choice for the folding model. The calculation of the density-dependent component of the Gogny interaction is trivial. In the case of the finite-range components (Yukawa or Gaussian), Eqs. (11) and (12) are solved by iteration. Some 20 iterations are needed to obtain convergence within eight significant digits at all radial distances.

A repulsive contact term is added to the heavy-ion potential to account for what we called in Ref. [10] "the incompressibility of nuclear matter." We adopted the following functional form:

$$V_{\rm comp}(R) = V_{\rm rep}\int d\boldsymbol{r}_1 d\boldsymbol{r}_2 \widetilde{\rho}_1(\boldsymbol{r}_1)\widetilde{\rho}_2(\boldsymbol{r}_2)\delta(\boldsymbol{R}+\boldsymbol{r}_1-\boldsymbol{r}_2), \qquad (14)$$

where the normalized density $\widetilde{\rho}(r)$ has a functional dependence identical to Eq. (1) but with a less diffusive surface and a slightly larger radius. The incompressibility required for the compound nucleus is calculated within the extended Thomas-Fermi model [31]: $K = 223.73$ MeV for $^{96}$Zr and $^{144}$Nd and $K = 226.55$ MeV for $^{84}$Kr.

There is a weak spurious energy dependence arising from the exchange part of the potential (11). We checked that the fusion cross section is little affected by this dependence.

In Fig. 1 the Coulomb + nuclear potential of the $^{48}$Ca + target is displayed at incident energy $E = 40$ MeV for $^{36}$S, 50 MeV for $^{48}$Ca, and 90 MeV for $^{96}$Zr. We note that the position and the height of the barrier is almost invariant for the four types of potentials for each projectile-target combination.

As a strategy to achieve a similar quality fit to the data for all three reactions, we kept fixed the diffuseness $a$ and half radii $c$ and $c_{\rm rep}$ used in the standard and modified densities and instead we varied $a_{\rm rep}$. For the matter density entering in the repulsive potential, we used for the diffuseness $a_{\rm rep}$ values ranging between 0.465 and 0.492 fm. Thus, a single parameter $a_{\rm rep}$ is varied within the nuclear potential to obtain the fit to the experimental cross section. The parameters of the heavy-ion potentials are listed in Tables I and II.

## III. CROSS-SECTIONS ANALYSIS

We calculate fusion cross section within a CC approach using a coupling scheme and physical input as described below. For $^{48}$Ca we include a $2^+$ state at 3.832 MeV from the quasiground band and a $3^-$ state from the octupole band at 4.507 MeV [32]. The corresponding Coulomb quadrupole deformation, $\beta_{2C} = 0.102$, is consistent with the deformations extracted from the experimental values of $B(E2)$ [33], whereas the Coulomb octupole deformation is taken $\beta_{3C} = 0.203$, also consistent with the recommended value [34]. The nuclear deformations are taken as $\beta_{2N} = 0.09$ and $\beta_{3N} = 0.16$.

For $^{36}$S we include a $2^+$ state at 3.291 MeV together with the $3^-$ state at 4.194 MeV. The corresponding Coulomb deformations, $\beta_{2C} = 0.163$ and $\beta_{3C} = 0.38$, are extracted from the reduced electric quadrupole transition probabilities given in the compilation [33] and the reduced electric-octupole transition probabilities from the compilation of Kibédi and Spear [34]. The corresponding nuclear deformations are $\beta_{2N} = 0.15$ and $\beta_{3N} = 0.3$.

TABLE II. Parameters of the heavy (H) and light (L) fragment densities and of the heavy-ion potentials for $^{36}$S + $^{48}$Ca and $^{96}$Zr + $^{48}$Ca.

| Interaction | $c_{\rm H}$ (fm) | $c_{\rm L}$ (fm) | $c_{\rm H,rep}$ (fm) | $c_{\rm L,rep}$ (fm) | $a_{\rm rep}$ (fm) | $V_{\rm rep}$ (MeV) | $V_{\rm min}$ (MeV) | $V_{\rm bar}$ (MeV) |
|---|---|---|---|---|---|---|---|---|
| | | | | $^{36}$S + $^{48}$Ca | | | | |
| M3Y-Reid | 3.75 | 3.40 | 3.93 | 3.5 | 0.479 | 6045 | 17.63 | 42.05 |
| M3Y-Paris | 3.75 | 3.40 | 3.93 | 3.5 | 0.475 | 6436 | 24.36 | 42.06 |
| D1S | 3.75 | 3.40 | 3.93 | 3.5 | 0.477 | 12903.7 | 28.86 | 42.05 |
| D1N | 3.75 | 3.40 | 3.93 | 3.5 | 0.475 | 13478 | 26.75 | 42.16 |
| | | | | $^{96}$Zr + $^{48}$Ca | | | | |
| M3Y-Reid | 3.75 | 4.83 | 3.93 | 4.55 | 0.47 | 6404.4 | 22.15 | 95.07 |
| M3Y-Paris | 3.75 | 4.83 | 3.93 | 4.55 | 0.465 | 6732.3 | 51.55 | 95.33 |
| D1S | 3.75 | 4.83 | 3.93 | 4.55 | 0.492 | 12789.9 | 38.88 | 95.24 |
| D1N | 3.75 | 4.83 | 3.93 | 4.55 | 0.487 | 13187.4 | 13.70 | 95.18 |

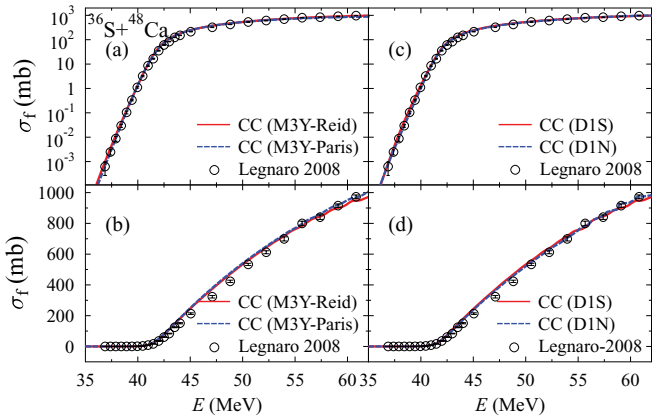


FIG. 2. (Color online) Fusion cross sections for the system $^{36}$S + $^{48}$Ca compared to the experimental data of Ref. [1] (circles). In (a) and (c) the cross sections are represented in logarithmic scale, whereas in (b) and (d) the representation is made in linear scale.

In the case of $^{96}$Zr we take a $2^+$ state at 1.751 MeV with Coulomb deformations $\beta_{2C} = 0.08$ and a $3^-$ state at energy 1.897 MeV with corresponding deformation $\beta_{3C} = 0.28$. A similar input was used in Ref. [5], however, assuming that $\beta_C = \beta_N$. Our choice was $\beta_{2N} = 0.1$ and $\beta_{3N} = 0.30$.

We include only one-phonon excitations in $^{36}$S and $^{48}$Ca and two-phonon excitations in $^{96}$Zr for the octupole states. As for the quadrupole states we include two-phonon excitation for all three nuclei. Mutual excitations are included as well, according the prescription described in Refs. [35,36].

In Figs. 2–4 we compare the cross sections of the three fusing systems to the experimental data. In the top panels the cross sections are given in logarithmic scale, whereas in the bottom panels we display the cross sections in linear scale. Also, it proved to be unnecessary to introduce dissipation via an imaginary potential.

To discriminate between the interactions we plot in Fig. 5 the ratio of experimental to theoretical cross section. For $^{36}$S + $^{48}$Ca the ratio is close to 1 throughout the entire range of energies. Though there are apparently no major differences between the four interactions, a slightly better agreement in the

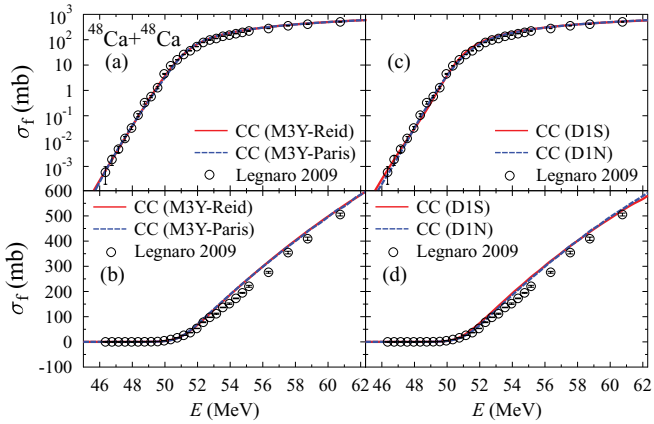


FIG. 3. (Color online) Same as in Fig. 2 for the system $^{48}$Ca + $^{48}$Ca compared to the experimental data of Ref. [2] (circles).

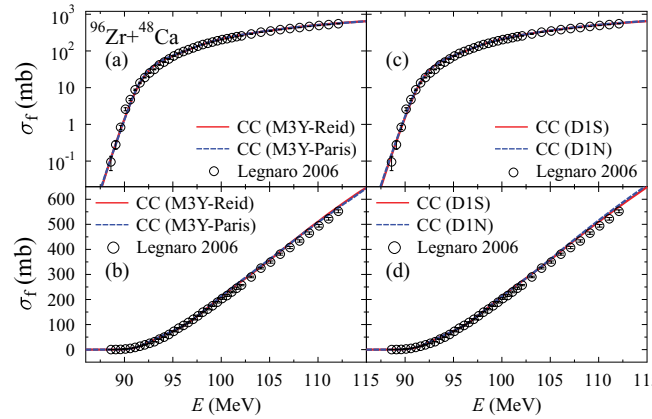


FIG. 4. (Color online) Same as in Fig. 2 for the system $^{96}$Zr + $^{48}$Ca compared to the experimental data of Ref. [5] (circles).

low-energy region when using the interaction M3Y-Paris can be remarked. Above the barrier all four interactions provide similar values of the ratio. At approximately 1 MeV below the barrier (≈42 MeV) a weak maximum of $\sigma_{\rm exp}/\sigma_{\rm th}$ is developing.

For the reaction, $^{48}$Ca + $^{48}$Ca, the two M3Y parametrizations are obviously providing a better agreement to the data compared to the two Gogny parametrizations below the Coulomb barrier. There are clearly two maxima developing slightly under the barrier. Note that for this reaction, a strong peak at the same energy (≈50 MeV) was also found in

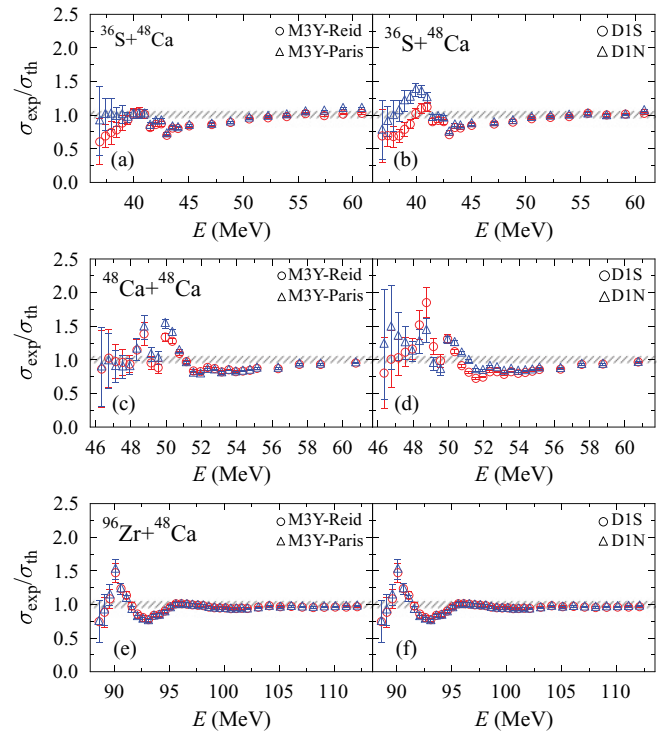


FIG. 5. (Color online) Experimental to theoretical cross sections ratios for $^{36}$S + $^{48}$Ca [panels (a) and (b)], $^{48}$Ca + $^{48}$Ca [panels (c) and (d)], and $^{96}$Zr + $^{48}$Ca [panels (e) and (f)]. The thin hatched region is centered around ratio equal to 1.

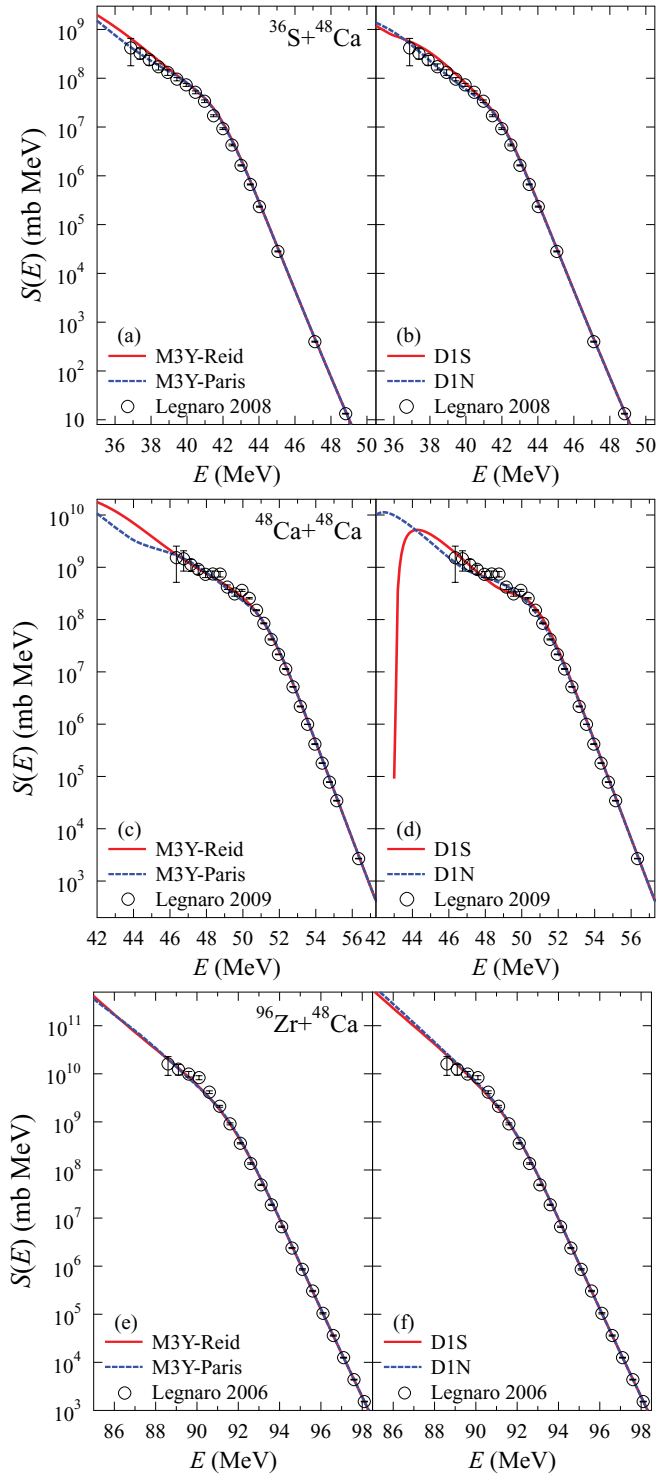


FIG. 6. (Color online) Calculated $S$ factors for the systems $^{36}$S + $^{48}$Ca [panels (a) and (b)], $^{48}$Ca + $^{48}$Ca [panels (c) and (d)], and $^{96}$Zr + $^{48}$Ca [panels (e) and (f)] are compared to the experimental data of Refs. [1,2], and [5].

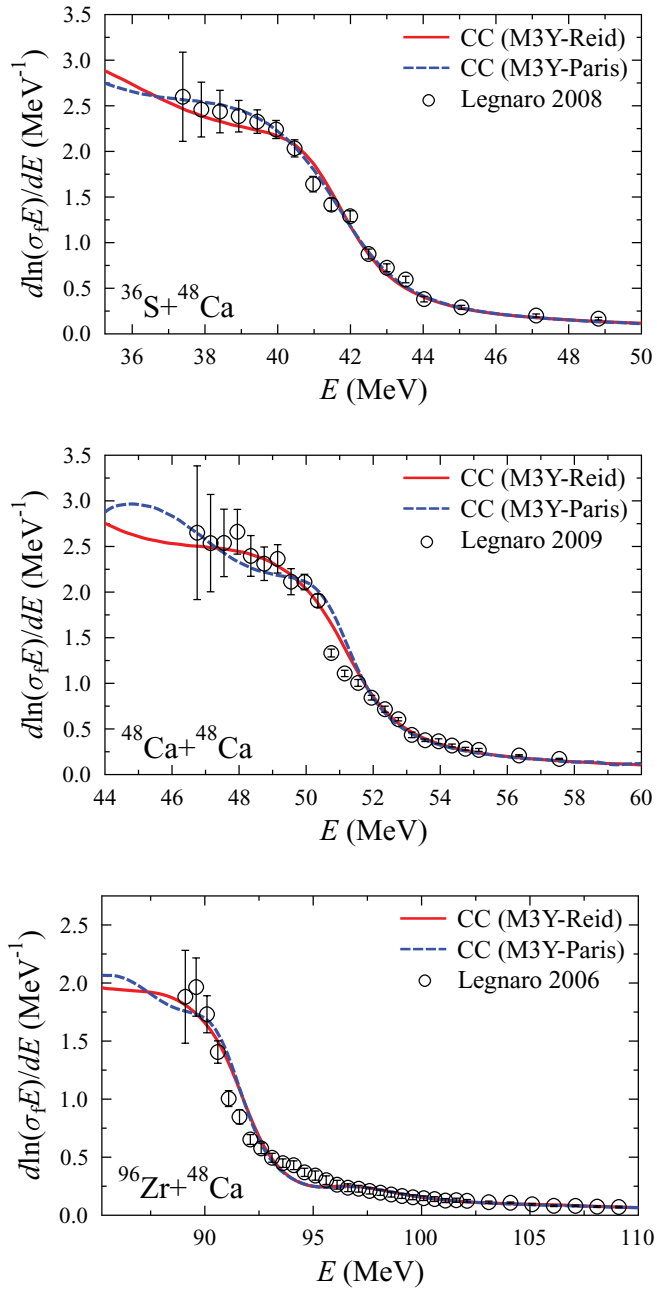


FIG. 7. (Color online) Calculated logarithmic derivatives $d\ln(\sigma_f E)/dE$ for the three systems $^{36}$S + $^{48}$Ca, $^{48}$Ca + $^{48}$Ca, and $^{96}$Zr + $^{48}$Ca compared to the experimental data of Refs. [1] and [2]. Numerical derivatives are calculated by a five-point formula.

Ref. [37]. However, in our description for the lowest data points we obtain values of the ratio closer to the ideal value 1.

For the third reaction, $^{96}$Zr + $^{48}$Ca, all four interactions are producing a very similar description of the data. Near the barrier, we observe oscillations of the ratio, with a more pronounced maximum at ≈90 MeV.

The calculated astrophysical factor $S(E) = \sigma_f(E)Ee^{2\pi\eta}$, where $\eta(E) = Z_1Z_2e^2\sqrt{\mu/(2\hbar^2E)}$, is the Sommerfeld parameter at c.m. energy $E$, is displayed and compared to the data in Fig. 6 for the three systems. For $^{36}$S + $^{48}$Ca the calculated $S$ factor deviates from experiment in the low-energy sector for the interactions M3Y-Reid and Gogny-D1S. For the reaction $^{48}$Ca + $^{48}$Ca we find that both M3Y interactions are providing a better description of the data. No maximum in the $S$ factor develops under the barrier. For the last reaction, $^{96}$Zr + $^{48}$Ca,

this conclusion is clearly confirmed for all four interactions (see Fig. 6, bottom panel).

The logarithmic derivatives calculated with M3Y forces, $L(E) = d\ln(E\sigma_f)/dE$, are compared with the experiment in Fig. 7. This representation has the advantage compared to the $S$-factor representation that it is more sensitive in the sub-barrier region. The deviations from the experimental data mirror the irregularities already encountered in the ratio $\sigma_{exp}/\sigma_{theor}$. Our calculation confirms the conclusion reached earlier by the Legnaro group; that is, well below the Coulomb barrier $L(E)$ levels off. In the case of $^{96}Zr + ^{48}Ca$, it was pointed out in Ref. [5] that the data "probably show the expected low-energy plateau below $E \sim 90$ MeV."

A last point that we would like to discuss is related to the observation made in Ref. [2] that the experimental logarithmic slopes of the systems $^{36}S$ and $^{48}Ca + ^{48}Ca$, plotted as a function of the cross section, are very similar despite the different sign of the $Q$ value and different reduced masses. In Fig. 8 we plot this unusual representation of fusion data and compare them with our calculated cross sections. The theoretical curves are also scaling in a very similar way. In our view the most probable physical explanation of this result is the corresponding scaling of the fusion barriers. In the inset of Fig. 8 we represent the barriers of these systems for two of the interactions earlier plotted in Fig. 1, this time as a function of the proximity distance $s = r - R_1 - R_2$ instead of the fragment-fragment distance $r$. Both potentials are normalized to the barrier heights, which we read off from Tables I and II, and the nuclear radii are taken as $R_1$ ($^{36}S$) = 3.31 fm and $R_2$ ($^{48}Ca$) = 3.53 fm. We remark that the barriers are also nicely scaling together above energies where the cross sections approach the $\mu$b values. Consequently, we infer the similarity between the two logarithmic slopes as a result of the proximity property of the double-folding heavy-ion potentials [38]. The quantum tunneling governing the fusion for sub-barrier energies, takes

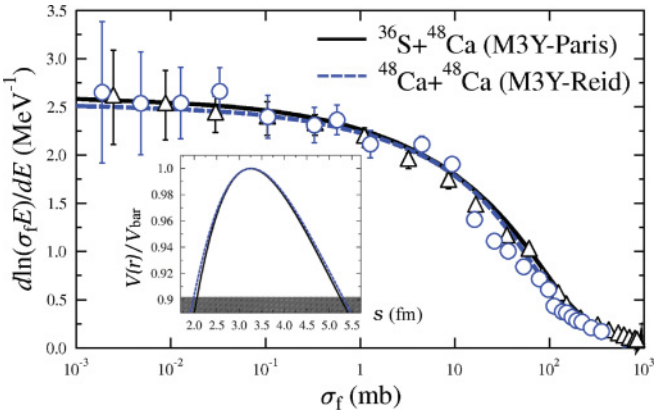


FIG. 8. (Color online) Experimental logarithmic slope versus cross section for the systems $^{36}S + ^{48}Ca$ (open triangles from Ref. [1]) and $^{48}Ca + ^{48}Ca$ (open circles from Ref. [2]) compared to theoretical calculations using the M3Y-Paris interaction for the first system (black solid line) and the M3Y-Reid interaction for the second one. In the inset the corresponding potentials normalized to the barrier heights for the two systems are represented versus the proximity distance $s$. The shaded region corresponds to bombarding energies where the cross sections are dropping below $10^{-3}$ mb.

place across very similar barriers. At such low energies nuclear structure effects play a minor role.

## IV. CONCLUSIONS

In this paper we analyzed three fusion reactions involving $^{48}Ca$ as projectile-target and displaying hindrance at energies well below the Coulomb barrier. A common feature of these systems is that the experimental logarithmic derivative, after a sharp increase just below the Coulomb barrier, apparently develops a plateau with decreasing cross section as a function of the energy. Obviously, this feature is in contrast to other fusing systems for which it was concluded that the slopes have a pronounced diverging behavior with decreasing energy, the most notorious cases being $^{58}Ni + ^{58}Ni$ and $^{64}Ni + ^{64}Ni$ [39].

The heavy-ion potential for these fusion reactions is based on microscopic $G$-matrix $N$-$N$ effective interactions, as well on interactions well tested in HFB calculations. As a result double-folding potentials including direct knock-on exchange and a repulsive component, which prevents strong density overlaps in the compound system, lead to similar barrier properties (position, height, thickness).

The hindrance at sub-barrier energies is consistently described by keeping the same nuclear structure input for the nucleus $^{48}Ca$ in all three reactions. Moreover, the parameters of the nuclear-matter densities for the three nuclei are predicting rms radii in close agreement with the values recommended by nuclear data compilations and the Coulomb quadrupole deformations are extracted from experimental $B(E\lambda)$ values. These features ensure an equally good description of fusion cross section in both low- and high-energy sectors.

From the analysis of the ratio of the measured to the calculated cross section we infer the existence of oscillations of this quantity near the barrier, almost independent of the interaction used in the model. Although we have for the time being no explanation, the origin of this phenomenon could be traced back to the limitations of the reaction model employed in this paper rather than the imprecise measurement of the cross section. The measured cross section has a weak tendency for a resonant behavior under the barrier, similar, though in a less enhanced manner, to the case of the evaporation cross section of $^{12}C + ^{12}C$ [23]. The ratio of the measured to the calculated cross section allows us to conclude that for the reaction $^{48}Ca + ^{48}Ca$ the M3Y-Reid and -Paris interactions produce a better fit to the data compared to the Gogny-D1S and D1N. This is quite surprising owing the ambiguity in the short-range behavior of the odd components (SO, TO) and the absence of any density dependence in these interactions. Instead, for the case $^{36}S + ^{48}Ca$ M3Y-Paris performs better in the extreme sub-barrier region than M3Y-Reid. For the case $^{96}Zr + ^{48}Ca$ the four employed interactions describe equally well the data.

The only case where we obtain a clear maximum for the astrophysical $S$ factor is $^{48}Ca + ^{48}Ca$ with D1S interaction, but the corresponding fit is less good compared to other interactions. For all other cases the $S$ factor continues to increase below the last measured cross section. Therefore, we agree with the conclusion reached by the Legnaro group for

the reactions $^{36}$S, $^{48}$Ca + $^{48}$Ca (see, for example, Ref. [6]) that no maximum develops in the $S$ factor at extreme sub-barrier energies. For $^{96}$Zr + $^{48}$Ca, though the data do not show clearly this effect, our calculations suggest that also no maximum develops in the $S$ factor. Consequently, we do not confirm the appearance of such a maximum, as predicted in Refs. [19,37], nor a continuous sharp increase of the logarithmic derivative with decreasing cross section.

Finally, we would like to reiterate that the paramount role played by quantum tunneling in sub-barrier fusion is illustrated also by the nice overlap between the logarithmic derivatives of the systems $^{36}$S and $^{48}$Ca + $^{48}$Ca versus $\sigma_f$.

Before ending it is worthwhile to comment on the limitations and possible improvements of the reaction model used in this paper. The local equivalent potential of the nonlocal kernel arising from antisymmetrization of the matrix elements was obtained in the lowest order of Perey-Saxon approximation. In the future we think we should examine higher-order corrections to this approach. It may be also appropriate to extend the range of the $N$-$N$ effective interactions by including in the calculations other fundamental density dependent $G$-matrix interactions to better understand the role of density dependence. One should also test the influence of an absorptive component in the optical model potential because nucleon breakup and neutron transfer may play a role at sub-barrier energies. For consistency it is necessary to derive the strength of the repulsive component from an equation of state generated by the effective interaction itself, at least at the Hartree-Fock level. Another possible improvement concerns the calculation of the transition operator in the CC method using the density fluctuations corresponding to the excitation of phonon states beyond the Tassie model.

## ACKNOWLEDGMENTS

We are grateful to A. M. Stefanini for providing tabulated cross sections data for the reactions $^{36}$S + $^{48}$Ca and $^{48}$Ca + $^{48}$Ca and to C. Matei for assistance with the artwork. This work received support from CNCSIS Romania, under Program No. PN-II-PCE-2007-1, Contract No. 49.

[1] A. M. Stefanini *et al.*, Phys. Rev. C **78**, 044607 (2008); G. Montagnoli *et al.*, AIP Conf. Proc. **1098**, 38 (2009).
[2] A. M. Stefanini *et al.*, Phys. Lett. B **679**, 95 (2009); F. Scarlassara *et al.*, AIP Conf. Proc. **1165**, 375 (2009).
[3] M. Trotta, A. M. Stefanini, L. Corradi, A. Gadea, F. Scarlassara, S. Beghini, and G. Montagnoli, Phys. Rev. C **65**, 011601 (2001).
[4] C. L. Jiang *et al.*, Phys. Rev. Lett. **89**, 052701 (2002).
[5] A. M. Stefanini *et al.*, Phys. Rev. C **73**, 034606 (2006).
[6] G. Montagnoli *et al.*, Phys. Rev. C **82**, 064609 (2010).
[7] K. Hagino, N. Rowley, and M. Dasgupta, Phys. Rev. C **67**, 054603 (2003).
[8] N. Rowley and K. Hagino, Nucl. Phys. A **834**, 110c (2010).
[9] J. O. Newton *et al.*, Phys. Lett. B **586**, 219 (2004).
[10] Ş. Mişicu and H. Esbensen, Phys. Rev. Lett. **96**, 112701 (2006).
[11] Ş. Mişicu and H. Esbensen, Phys. Rev. C **75**, 034606 (2007).
[12] H. Esbensen and Ş. Mişicu, Phys. Rev. C **76**, 054609 (2007).
[13] C. L. Jiang *et al.*, Phys. Lett. B **640**, 18 (2006).
[14] C. L. Jiang *et al.*, Phys. Rev. C **78**, 017601 (2008).
[15] P. O. Hess, Ş. Mişicu, W. Greiner, and W. Scheid, J. Phys. G **26**, 1 (2000).
[16] T. Ichikawa, K. Hagino, and A. Iwamoto, Phys. Rev. Lett. **103**, 202701 (2009).
[17] M. Dasgupta, D. J. Hinde, A. Diaz-Torres, B. Bouriquet, C. I. Low, G. J. Milburn, and J. O. Newton, Phys. Rev. Lett. **99**, 192701 (2007).
[18] A. S. Umar and V. E. Oberacker, Eur. Phys. J. A **39**, 243 (2009).
[19] H. Esbensen and C. L. Jiang, Phys. Rev. C **79**, 064619 (2009).
[20] J. W. Negele, Phys. Rev. C **1**, 1260 (1970).
[21] I. Angeli, Heavy Ion Phys. **8**, 23 (1998).
[22] G. F. Bertsch, J. Borysowicz, H. McManus, and W. G. Love, Nucl. Phys. A **284**, 399 (1977).
[23] Ş. Mişicu and F. Carstoiu, Nucl. Phys. A **834**, 180c (2010).
[24] N. Anantaraman, H. Toki, and G. F. Bertsch, Nucl. Phys. A **398**, 269 (1984).
[25] C. L. Jiang, K. E. Rehm, B. B. Back, and R. V. F. Janssens, Phys. Rev. C **75**, 015803 (2007)
[26] J. F. Berger, M. Girod, and D. Gogny, Nucl. Phys. A **502**, 85c (1989).
[27] F. Chappert, M. Girod, and S. Hilaire, Phys. Lett. B **668**, 420 (2008).
[28] X. Campi and D. W. L. Sprung, Nucl. Phys. A **194**, 401 (1972).
[29] F. Carstoiu and M. Lassaut, Nucl. Phys. A **597**, 269 (1996).
[30] D. T. Khoa, Phys. Rev. C **63**, 034007 (2001).
[31] W. D. Myers and W. J. Swiatecki, Nucl. Phys. A **601**, 141 (1996).
[32] M. Sakai and A. C. Rester, At. Data Nucl. Data Tables **20**, 441 (1977).
[33] S. Raman, C. W. Nestor, S. Kahane, and K. H. Bhatt, At. Data Nucl. Data Tables **42**, 1 (1989).
[34] T. Kibédi and R. H. Spear, At. Data Nucl. Data Tables **80**, 35 (2002).
[35] H. Esbensen and S. Landowne, Phys. Rev. C **35**, 2090 (1987).
[36] H. Esbensen, Prog. Theor. Phys. Suppl. **154**, 11 (2004).
[37] H. Esbensen, C. L. Jiang, and A. M. Stefanini, Phys. Rev. C **82**, 054621 (2010).
[38] D. M. Brink and F. Stancu, Nucl. Phys. A **299**, 321 (1978).
[39] C. L. Jiang *et al.*, Phys. Rev. Lett. **93**, 012701 (2004).